Intrinsic Vacancy-Induced Nanoscale Wire Structure in Heteroepitaxial Ga$_2$Se$_3$/Si(001)

Taisuke Ohta,[1,*] D. A. Schmidt,[2] Shuang Meng,[2,†] A. Klust,[2,‡] A. Bostwick,[2,*] Q. Yu,[2]
Marjorie A. Olmstead,[2] and F. S. Ohuchi[1,§]

[1]*Department of Materials Science and Engineering, University of Washington, Box 352120, Seattle, Washington 98195, USA*
[2]*Department of Physics, University of Washington, Box 351560, Seattle, Washington 98195, USA*
(Received 15 December 2004; published 22 March 2005)

A highly anisotropic growth morphology is found for heteroepitaxial gallium sesquiselenide (Ga$_2$Se$_3$) on the lattice matched substrate, arsenic-terminated Si(001). Scanning tunneling microscopy of Ga$_2$Se$_3$ films reveals nanoscale, wirelike structures covering the surface in parallel lines, less than 1 nm wide and up to 30 nm long. Core-level photoemission spectroscopy and diffraction reveals the local structure of buried Ga and Se atoms to reflect the bulk, defected zinc-blende structure of β-Ga$_2$Se$_3$, which contains ordered $\langle 110 \rangle$ arrays of Ga vacancies. These ordered vacancy lines are proposed to be responsible for the observed growth anisotropy in heteroepitaxial Ga$_2$Se$_3$.

PACS numbers: 68.37.Ef, 68.55.−a

The intrinsic structural vacancies of semiconducting chalcogenides lead to numerous interesting structural, electronic, and optical properties. In this Letter, we demonstrate a new mechanism for creating a highly anisotropic growth morphology based on these ordered, intrinsic vacancies. In particular, we observe a nanoscale wirelike morphology of gallium sesquiselenide (Ga$_2$Se$_3$) grown heteroepitaxially on arsenic-terminated Si(001) [Si(001):As] that extends in the same direction for several layers. Growth anisotropy has been observed in a number of semiconductor epitaxial systems, and has been exploited to form technologically important self-assembled nanostructures [1]. In these systems, the anisotropic growth has been attributed to a number of factors, including kinetic, thermodynamic, defect, and strain effects. For example, in Si(001) homoepitaxy, one-dimensional islands composed of Si-Si dimers are formed through a higher sticking coefficient at the end of dimer rows than along their sides, but the next layer alternates in direction [2]. Nanoscale dots and clusters are often formed by defects and/or strains generated at the heterointerface, among which InGaAs nanodots on GaAs [3] and SiGe clusters on Si [4] are the systems most thoroughly investigated. With the lattice constant of Ga$_2$Se$_3$ very close to that of Si [5], the anisotropic growth of Ga$_2$Se$_3$ is controlled not by strain, but rather by its anisotropic structural vacancies. Anisotropic growth driven by intrinsic structural vacancies has not, to our knowledge, been previously observed; its understanding opens new opportunities for controlled growth of nanoscale structures in other materials.

In bulk Ga$_2$Se$_3$, the competition between the tetrahedral sp^3 bonding, characteristic of Ga in III−V and Se in II−VI semiconductors, and the extra electron per the cation-anion pair (nine valence electrons, instead of eight) results in intrinsic structural vacancies. Ga$_2$Se$_3$ crystallizes in a defected zinc-blende (ZB) structure with one-third of the cation (Ga) sites vacant; in β-Ga$_2$Se$_3$, these sites are ordered along $\langle 110 \rangle$ lines [6]. Ordered vacancy arrays yield anisotropic optical transmission and photoluminescence

[7,8], and are theoretically predicted to result in a non-dispersing, valence band maximum along the $\langle 110 \rangle$ vacancy-line direction [6]. Interest in utilizing β-Ga$_2$Se$_3$ in optoelectronics has led to study of its epitaxial growth on GaP [7,9] and GaAs [10], where Se diffusion into the substrate has been suggested to play a key role in initiating growth. Heteroepitaxy of Ga$_2$Se$_3$ on Si is expected to differ significantly from growth on Ga-containing substrates, and to display the intrinsic growth nature of this highly anisotropic material in the absence of long-range Se interdiffusion.

In this Letter, we investigate heteroepitaxial growth of Ga$_2$Se$_3$ on Si(001):As using *in situ* scanning tunneling microscopy (STM), high resolution core-level photoemission spectroscopy (PES), and x-ray photoelectron diffraction (XPD). PES and XPD reveal Ga and Se atoms to be in a defected ZB structure, and STM reveals nanoscale, nonmetallic, wirelike structures aligned on the surface. The average spacing between the wire structures matches the spacing between vacancy lines in β-Ga$_2$Se$_3$, and the orientation of the wire structure is strongly influenced by the Si(001):As-dimer row direction. We address atomistic processes at the growth front, and discuss their correlation with vacancy arrays in β-Ga$_2$Se$_3$.

Experiments were carried out both at the Advanced Light Source (ALS), Beamline 7.0.1, for high resolution core-level PES using synchrotron radiation and XPD using Mg $K\alpha$ x-ray ($h\nu$ = 1253.6 eV), and in Seattle, for ultra-high vacuum scanning probe microscopy [11]. Boron-doped Si(001) substrates (1 Ω cm for PES and XPD, 0.02–0.1 Ω cm for STM) were chemically treated to form a thin oxide layer prior to introduction into the UHV chamber, degassed at ~550 °C for >12 h, and flashed at 1200 °C to obtain a well ordered 2 × 1 reconstruction. To avoid unwanted Si-Se reactions [12–14], the Si(001) substrate was terminated by one monolayer of arsenic by exposing clean Si(001) to As$_4$ at substrate temperature T_{sub} = 720–800 °C, cooling slowly in the As$_4$ flux to T_{sub} = 350 °C, and then pumping out the As$_4$ before cool-

116102-1

ing the sample to room temperature. Long- and short-range sample uniformity was confirmed by low energy electron diffraction (LEED) and STM. Sample temperatures were measured using an infrared pyrometer.

Ga_2Se_3 deposition utilized a GaSe Knudsen cell, either alone (in Seattle) or in combination with additional Se from an electrochemical cell (in ALS) [15]. During deposition, sample temperatures were $T_{sub} = 470\,°C$ for the photoemission experiments, and covered a range of deposition temperatures for STM (sample for Fig. 1 grown at $T_{sub} = 525\,°C$). Samples prepared by both methods exhibit characteristic LEED patterns of weak 1×1 with additional long streaks partly connecting the 1×1 spots [Fig. 1(g)]. Film thicknesses were estimated from the ratio of Se $3d$ to Si $2p$ peaks using Mg $K\alpha$ x-ray photoelectron spectroscopy, calibrated against a single GaSe bilayer on Si(111) [16]. All measurements were carried out at room temperature. STM images and XPD projections presented here are oriented with the Si substrate $\langle 110 \rangle$ direction toward the top.

The strongly anisotropic growth of Ga_2Se_3 on Si(001):As is seen clearly in Fig. 1. Figure 1(a) shows a three-dimensional (bird view) representation of the surface of a 0.9 nm (2 cubic unit cells [5]) Ga_2Se_3 film; Fig. 1(b) is the cross section between the white arrows in 1(a). Similar morphology was also observed on 0.6 and 1.1 nm films. The surface is covered with wirelike structures, several tens of nm long, with a homogenous width of less than 1 nm (finite STM tip size precludes a more accurate width measurement). The orientation of the wire structures alternates between vertical orientation (VO, [110]) and horizontal orientation (HO, [1$\bar{1}$0]) on a 50 nm length scale [Fig. 1(a)]. The average height difference between adjacent VO and HO regions is ~ 0.13 nm, and from one VO or HO region to the next similar region is about 0.26 nm

[Fig. 1(b)], corresponding to the height of single- and double-atomic steps on Si(001). The orientation of the Si(001) 2×1 surface unit cell also alternates by 90° with each single-height step, indicating a strong correlation between the Si dimer row orientation and that of the wires. Measurements at lower coverages show the wires to be perpendicular to the Si(001):As-dimer rows [17].

Higher resolution (20×20 nm^2) STM images showing the atomic scale of the wire structure are shown in Figs. 1(c) and 1(e). There are four distinct height levels, differing by 0.26 nm, or a half cubic unit cell ($Ga_{2/3}$-Se bilayer) of β-Ga_2Se_3 [5]. The measured height difference is independent of the bias polarity, and was further confirmed by *in situ* noncontact scanning force microscopy. Along the wire structure, we observe atomic corrugation of height 0.01 nm with periodicity equal to the unreconstructed surface unit cell of β-Ga_2Se_3, $a_s = 3.87$ Å [5]. Identical atomic corrugations were observed along the wire structures at all four height levels. The atomic corrugation with a_s periodicity and bilayer height difference between different wires suggest each wire structure is terminated with the same species, Ga or Se, because the ZB structure has equivalent termination every half unit cell.

The average spacing between wire structures (or, equivalently, between trenches) at the same level is about 1.2 nm, or $\sim 3a_s$, which is the spacing between ordered vacancy lines in β-Ga_2Se_3. This typical spacing is indicated by the dashed lines in Fig. 1(e), and compared to the 0.76 nm spacing between Si(001) 2×1 dimer rows in Fig. 1(f). By comparing the lateral position of wire structures at the same level, we can see that adjacent wire structures approaching end to end may be shifted by half the dimer separation, a_s [see solid lines in the white circle in Fig. 1(e)]. This illustrates that two wires at the same level with their centers displaced by a_s cannot grow further
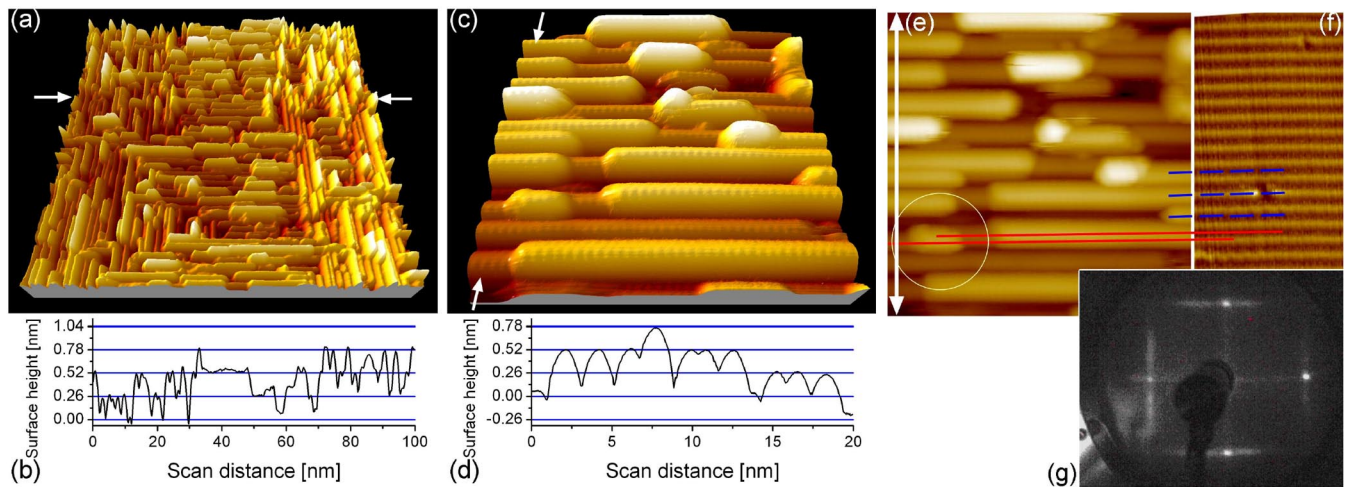

FIG. 1 (color online). Growth morphology of 0.9 nm thick Ga_2Se_3/As/Si(001). (a) The 100×100 nm^2 STM image (5.4 V, 0.09 nA), shown in 3D. (b) Cross section between white arrows in (a). (c) The 20×20 nm^2, image (-5.4 V, 0.09 nA), shown in 3D. (d) Cross section between the white arrows in (c) and (e). (e) Identical image to (c), shown in 2D. (f) Bare Si(001) 2×1 surface showing Si dimer rows at the same scale as (e), imaged at -4 V, 0.15 nA. (g) LEED pattern at electron energy $E_e = 40.3$ eV.

when they meet. Also notice that some wires grow on top of the wires at lower level.

This atomic corrugation and the surface morphology are consistent with the LEED pattern with streaks not extending over the entire Brillouin zone, but only about two-thirds of it is shown in Fig. 1(g): 1×1 spots are due to atomic corrugations of period a_s, and streaks to variable spacings between wire structures.

The element specific chemical environment and the crystal structure of the Ga_2Se_3 were studied using PES and XPD. A Se $3d$ core-level photoemission spectrum (taken at normal emission with $h\nu = 246$ eV photons), shown in Fig. 2(a), displays two chemical environments for Se atoms. A fit to spin-orbit split Voigt functions reveals two components separated by 0.92 eV, with intensity ratio ~2:1 between the higher binding energy and lower binding energy components. The splitting and intensity ratio between the two components is very similar to those for Se $3d$ emission from Ga_2Se_3 films grown on GaAs substrates by annealing in Se [18]. The Ga $3d$ spectrum [Fig. 2(b)] consists of a broad, main peak and a smaller peak at lower binding energy. Both the Ga and Se peak widths (about 0.9 eV) are significantly larger than our experimental resolution, with the Ga slightly broader than the Se. This indicates that there are multiple environments in the deposited thin film differing by only a small amount in binding energy.

Stereographic projections of the angle-dependent intensity of Mg $K\alpha$-excited Se and Ga $3d$ photoemission are shown in Figs. 2(c) and 2(d), respectively. At these high electron kinetic energies (~1200 eV), forward focusing dominates the XPD patterns [19]. For each projection, 1204 data points were sampled in a 120° azimuthal section and then subjected to a fourfold symmetrization to produce
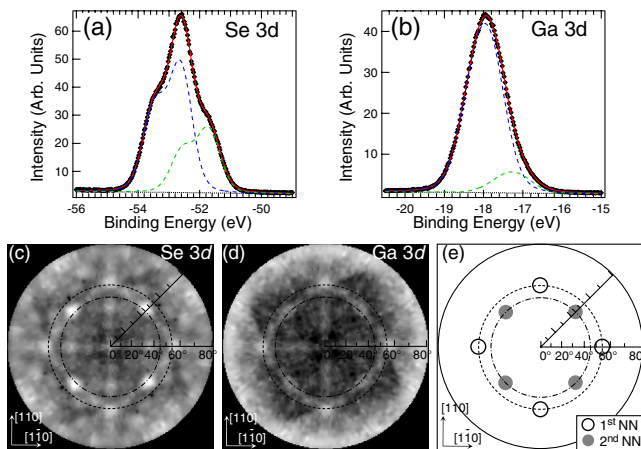
the 360° stereographic projection. At each data point, photoelectron intensities were measured in a 1 eV window near the peak center ($KE_{Se} = 1195$ eV, $KE_{Ga} = 1229$ eV), and at a reference point on the low binding energy side of each photoemission peak. The signals in Figs. 2(c) and 2(d) are the differences between the peak and background intensities.

Both the Ga $3d$ and the Se $3d$ emissions exhibit fourfold symmetry with strong diffraction spots within 1° of the nearest and next nearest neighbor directions in the ZB lattice [$\theta = 55°$ along $\langle 110 \rangle$ and $\theta = 45°$ along $\langle 100 \rangle$, respectively, highlighted in Fig. 2(e)]. For Se, the second nearest neighbor spots (scattering from Se) are more intense than the scattering from nearest neighbor Ga. For Ga, the inverse is true: scattering from nearest neighbor Se is more intense than that from next nearest neighbor Ga. These results indicate the Se and Ga form a defected ZB structure. The weaker intensity of the spots associated with forward scattering by Ga atoms may be attributed to having ~1/3 of the Ga sites vacant in the β-Ga_2Se_3 crystal structure.

The observed anisotropic morphology (or formation of wire structures) manifests a strongly anisotropic growth of Ga_2Se_3. The equality of the typical wire (or trench) spacing and the spacing between ordered vacancy arrays in β-Ga_2Se_3 (both $3a_s$) suggests the anisotropic surface morphology is strongly correlated to the vacancy ordering. Figure 3(a) shows a $\langle 110 \rangle$ projection of the β-Ga_2Se_3 crystal structure [6,20]. In the [001] direction (up), atomic sheets of Ga and Se alternate, with every third Ga site vacant in each Ga sheet. The vacancy sites continue normal to the paper, creating ordered vacancy arrays in the [110] direction. The vacancy lines stack to maximize their separation, so that all Se atoms are bonded to either 2 or 3 Ga atoms, and each vacancy array is lined by fully occupied Se lone-pair orbitals; the symmetric positioning also balances local dipoles. In Fig. 3(b), some of the atoms located above the vacancy in the middle of Fig. 3(a) are removed to illustrate a mechanism for wire structure formation.

Combining our knowledge of the bulk β-Ga_2Se_3 structure with our experimental results, we present an atomic structure model of the wire structure in Fig. 3(c). Wire structures are separated, on average, by $3a_s$, and the heights of the wire structures are increments of the half unit cell of β-Ga_2Se_3. The open space (trench) between the wire structures is equivalent to the vacancy array in

FIG. 2 (color online).   Photoemission spectroscopy and diffraction of 0.8 nm Ga_2Se_3 film. (a) Se $3d$ and (b) Ga $3d$ spectra with photon energy $h\nu = 246$ eV, normal emission. (c) Se $3d$ and (d) Ga $3d$ scanned angle stereographic projections of photoemission intensities with photon energy 1253 eV (Mg $K\alpha$ x-ray source). (e) Characteristic angles for the first nearest and second nearest neighbor directions in a ZB lattice.
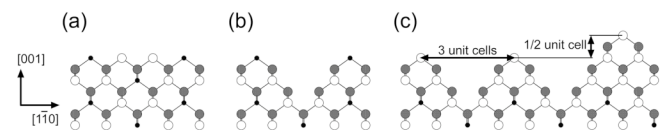

FIG. 3.   Atomic structural model for wire structure. (a) $\langle 110 \rangle$ projection of ideal β-Ga_2Se_3 crystal; (b) some atoms removed from (a); (c) the morphology of wire structures. Open circles denote Ga atoms, gray circles Se atoms, and small filled circles vacancies.

β-Ga_2Se_3. The identity of the topmost atom as Ga is inferred from the perpendicular relationship between the wire structures and the underlying As-dimer rows, assuming the stacking is the expected Si-Ga-Se-Ga. This is further confirmed by PES measurements as a function of thickness, where As-Si bonding at the interface is replaced by Ga-Si bonding as coverage increases, and by XPD showing arsenic atoms to occupy sites equivalent to Se atoms. Understanding of the interface formation and the nucleation process are required to elucidate the role and the locations of arsenic atoms. These results will be reported elsewhere [17].

The wire structure side walls are $(\bar{1}\,\bar{1}\,\bar{1})$ zinc-blende microfacets, i.e., hexagonal sheets of Se atoms. We observe no states near the Fermi level with either PES or STM, indicating no partially occupied surface orbitals at or near the surface. We attribute this absence of dangling bonds to the unique electron counting of this defected ZB structure. The tetrahedral bonding is satisfied by three Ga valence electrons $(4s^2 4p)$, and 5 of the 6 Se valence electrons $(4s^2 4p^4)$, leaving one extra electron to fill the Se dangling bond, creating a fully occupied lone-pair orbital. This fully occupied orbital stabilizes the hexagonal Se sheets and results in a chemically inert surface. We presume this leads to the observed anisotropic growth or formation of wire structures by lowering the adatom sticking coefficient on the side walls, so that adatoms rather migrate to the ends of the wire structure and extend its length. In a bulk β-Ga_2Se_3 crystal, the vacant Ga site is filled with four fully occupied lone-pair orbitals of adjacent Se atoms [20]. In these homogeneous wire structures, we expect the vacancies to be distributed such that they maintain local charge neutrality within the film. Thus, the individual vacancy location is determined by the local structures of the surface morphology, and may evolve with film thickness.

In conclusion, a new mechanism of anisotropic growth due to materials intrinsic structural vacancy is reported for Ga_2Se_3 heteroepitaxy on Si(001):As. The crystal structure of the thin film is determined to be defected zinc-blende Ga_2Se_3 by high resolution core-level PES and XPD. STM reveals narrow, semiconducting, wirelike structures several tens of nanometers long with 3 unit cells spacing. Based on the PES/XPD and the STM results, we presented a model atomic structure of the observed wirelike structures derived from vacancy ordering in β-Ga_2Se_3. The anisotropic growth of Ga_2Se_3 is attributed to the fully occupied lone-pair orbitals of Se atoms located on the side walls of the wire structure, leading to adatom attachment at the ends of the wires rather than on their sides. Wire growth is stopped by coalescence to other wires or atomic steps of the substrate. We conclude that structural vacancies in the Ga_2Se_3 crystal drive its highly anisotropic growth morphology.

*Present address: Advanced Light Source, Lawrence Berkeley National Laboratory, Berkeley, CA.
†Present address: Micron Technology, Inc., M.S. 1-719, Boise, ID.
‡Present address: Department of Chemical Engineering, Stanford University, Stanford, CA.
§Electronic address: ohuchi@u.washington.edu

[1] *Low-Dimensional Semiconductor Structures, Fundamentals and Device Applications*, edited by K. Barnham and D. Vvedensky (Cambridge University Press, Cambridge, 2001).
[2] C. Pearson, M. Krueger, and E. Ganz, Phys. Rev. Lett. **76**, 2306 (1996).
[3] See, for example, S. Guha *et al.*, Appl. Phys. Lett. **57**, 2110 (1990); M. Krahl *et al.*, Appl. Phys. Lett. **61**, 813 (1992); C. W. Snyder *et al.*, Phys. Rev. B **46**, 9551 (1992).
[4] F. K. LeGoues *et al.*, Phys. Rev. B **42**, 11 690 (1990); Y.-W. Mo *et al.*, Phys. Rev. Lett. **65**, 1020 (1990); D. J. Eaglesham and M. Cerullo, Phys. Rev. Lett. **64**, 1943 (1990).
[5] Lattice constants of Ga_2Se_3 and Si are $a = b = 5.48$ Å, $c = 5.41$ Å, and $a_{Si} = 5.43$ Å, respectively. Surface unit cell of Ga_2Se_3 is $a_s = a/\sqrt{2} = 3.87$ Å.
[6] M. Peressi and A. Baldereschi, J. Appl. Phys. **83**, 3092 (1998).
[7] A. Yamada *et al.*, Jpn. J. Appl. Phys. **31**, L186 (1992); T. Okamoto *et al.*, Jpn. J. Appl. Phys. **31**, L143 (1992).
[8] M. Ishikawa and T. Nakayama, Physica (Amsterdam) **17E**, 185 (2003).
[9] N. Teraguchi *et al.*, Appl. Phys. Lett. **59**, 567 (1991).
[10] See, for example, D. Li *et al.*, J. Vac. Sci. Technol. B **9**, 2167 (1991); F. S. Ohuchi and M. A. Olmstead, in *Wiley Encyclopedia of Electrical and Electronics Engineering*, edited by J. G. Webster (Wiley, New York, 1999), Vol. 19, p. 147.
[11] Omicron Nanotechnology GmbH, Germany.
[12] S. Meng, Ph.D. dissertation, University of Washington, 2000.
[13] R. D. Bringans *et al.*, Phys. Rev. B **45**, 13 400 (1992).
[14] C. Chauvet *et al.*, Appl. Phys. Lett. **73**, 957 (1998).
[15] A GaSe Knudsen cell creates Ga_2Se and Se_2 flux, and a Se electrochemical cell, Se_2 flux. For details, see [12] and A. Ludviksson *et al.*, J. Cryst. Growth **151**, 114 (1995).
[16] S. Meng *et al.*, Phys. Rev. B **61**, 7215 (2000); **64**, 235314 (2001).
[17] T. Ohta, Ph.D. dissertation, University of Washington, 2004; T. Ohta *et al.* (to be published).
[18] See, for example, D. R. Menke *et al.*, J. Vac. Sci. Technol. B **9**, 2171 (1991); C. Gonzalez *et al.*, J. Phys. Condens. Matter **16**, 2187 (2004).
[19] S. A. Chambers, Surf. Sci. Rep. **16**, 261 (1992); C. S. Fadley, Surf. Sci. Rep. **19**, 231 (1993).
[20] M. Ishikawa, Ph.D. dissertation, Chiba University, 1998.